Manifold SLIC: A Fast Method to Compute Content-Sensitive Superpixels

Yong-Jin Liu, Cheng-Chi Yu*, Min-Jing Yu*
Tsinghua University, China
{liuyongjin,ycc13,yumj14}@tsinghua.edu.cn

Ying He
Nanyang Technological University, Singapore
YHe@ntu.edu.sg

Abstract

Superpixels are perceptually meaningful atomic regions that can effectively capture image features. Among various methods for computing uniform superpixels, simple linear iterative clustering (SLIC) is popular due to its simplicity and high performance. In this paper, we extend SLIC to compute content-sensitive superpixels, i.e., small superpixels in content-dense regions (e.g., with high intensity or color variation) and large superpixels in content-sparse regions. Rather than the conventional SLIC method that clusters pixels in $\mathbb{R}^5$, we map the image I to a 2-dimensional manifold $\mathcal{M} \subset \mathbb{R}^5$, whose area elements are a good measure of the content density in I. We propose an efficient method to compute restricted centroidal Voronoi tessellation (RCVT) — a uniform tessellation — on M, which induces the content-sensitive superpixels in I. Unlike other algorithms that characterize content-sensitivity by geodesic distances, manifold SLIC tackles the problem by measuring areas of Voronoi cells on $\mathcal{M}$, which can be computed at a very low cost. As a result, it runs 10 times faster than the state-of-the-art content-sensitive superpixels algorithm. We evaluate manifold SLIC and seven representative methods on the BSDS500 benchmark and observe that our method outperforms the existing methods.

1. Introduction

Superpixels are perceptually meaningful atomic regions that can effectively capture image features and greatly reduce the complexity of subsequent image processing tasks, such as segmentation [10], contour closure [8], 2.1D sketches [21], object location [6], object tracking [19], stereo 3D reconstruction [14], and many others.

There are two major classes of algorithms to compute superpixels, namely, the graph-based methods and the clustering-based methods. Representing an image by a graph whose nodes are pixels, the graph-based algorithms minimize a cost function defined on the graph. Representative works include normalized cuts (NC) [16], the Felzenszwalb-Huttenlocher (FH) method [5], superpixel lattices (SL) [15], and the graph-cut-based energy optimization method (GraphCut) [17]. NC generates regular and compact superpixels, but does not adhere to image boundary and has a high computational cost — $O(N^{1.5})$ time complexity for an N-pixel image as observed in [9]. FH preserves boundary well and runs in $O(N \log N)$ time, but it produces superpixels with irregular sizes and shapes. Although SL runs in $O(N^{1.5} \log N)$ *theoretically*, it has an *empirical* time complexity $O(N)$, making it one of the fastest superpixel algorithms. However, their produced superpixels conform to grids rather than adhering to image boundaries. GraphCut is elegant and theoretically sound, but it is difficult to use due to many parameters involved in the algorithm.

The clustering-based algorithms group pixels into clusters (i.e., superpixels) and iteratively refine them until some convergence criteria are satisfied. Popular clustering methods are Turbopixels [9], simple linear iterative clustering (SLIC) [1] and structure-sensitive[1] superpixels (SSS) [18]. All three methods are initialized with a set of evenly distributed seeds $\{s_i\}_{i=1}^K$ in an image domain. They differ in the way of clustering. Turbopixels [9] generates a geometric flow for each seed and propagates them using the level set method. The superpixel boundary is the points where two flows meet. Although Turbopixels has a theoretical linear time complexity $O(N)$, computational results show that it runs slowly on real-world datasets [1]. SLIC [1] is an adaption of K-means that clusters pixels in a 5-dimensional Euclidean space combining colors and images. It assigns each pixel to a cluster of the nearest seed and iteratively updates the cluster center using centroidal Voronoi tessellation (CVT). SLIC is conceptually simple, easy to implement, and highly efficient in practice.

To compute content-sensitive superpixels, Wang et al. [18] adopted the geometric flow method [9] into a CVT optimization framework. A key difference between SSS and SLIC is that SLIC measures the distance between clusters

*C. Yu and M. Yu contributed equally to this paper

[1]Since in computer vision, "structure" is usually referred to as some high-order structures in the image, in this paper we use the word "content".

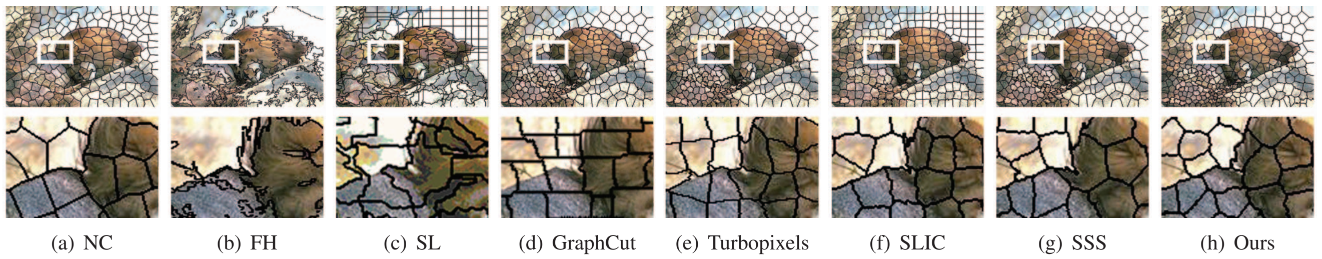

Figure 1. Superpixels obtained by normalized cuts (NC) [16], the Felzenszwalb-Huttenlocher (FH) method [5], superpixel lattices (SL) [15], the graph-cut-based energy optimization method (GraphCut) [17], turbopixels [9], simple linear iterative clustering (SLIC) [1], structure-sensitive superpixels (SSS) [18] and our method. Both FH and SL generate under segmentations in content-rich regions due to lack of compactness constraint, whereas the other methods produce regular superpixels. It is worth noting that only SSS and our method can produce content-sensitive superpixels. Our method outperforms the other methods in terms of under segmentation error, boundary recall and achievable segmentation accuracy. It also runs 10× faster than SSS, the state-of-the-art method for computing content-sensitive superpixels. See Section 6 for detailed comparison and discussion. Images are provided in high resolution for zoom-in examination.

using Euclidean distance whereas SSS takes geodesic distances into account. As a result, SLIC produces *uniform* superpixels everywhere, whereas SSS can effectively capture the non-homogenous feature in images, i.e., small superpixels in content-dense regions (e.g., with high intensity or color variation) and large superpixels in content-sparse regions. However, SSS is computationally expensive.

Inspired by the simplicity and high performance of SLIC [1] and the content-aware nature of SSS [18], we propose *manifold SLIC*, an extension of SLIC for fast computation of content-sensitive superpixels. Our key idea is to represent the image I as a 2-manifold $\mathcal{M}$ embedded in the combined color and image space $\mathbb{R}^5$, on which the area elements are a good measure of content density in I. We develop an efficient algorithm to compute restricted CVT — a uniform tessellation — on M, which induces the content-sensitive superpixels in I. Unlike other algorithms that characterize content-sensitivity by geodesic distances, manifold SLIC addresses the problem by measuring areas of Voronoi cells on $\mathcal{M}$, which can be computed at a very low cost. As a result, it runs 10 times faster than the state-of-the-art content-sensitive superpixels algorithm [18]. We evaluate manifold SLIC and seven representative methods on the BSDS500 benchmark and observe that our method outperforms the existing methods. See Figure 1.

2. Preliminaries

Since manifold SLIC is based on SLIC [1] and is also closely related to SSS [18], we briefly introduce both algorithms before presenting it.

2.1. SLIC

Let us denote by I the input image with N pixels. For a pixel $p \in I$, SLIC represents its color $\mathbf{c}(p)$ in the CIELAB color space, i.e., $\mathbf{c}(p) = (l(p), a(p), b(p))$. Given two pixels $p_1 = (u_1, v_1)$ and $p_2 = (u_2, v_2)$, SLIC measures the distance between them using a normalized Euclidean distance in the combined color and image space $\mathbb{R}^5$:

$$D(p_1, p_2) = \sqrt{\left(\frac{d_s}{N_s}\right)^2 + \left(\frac{d_c}{N_c}\right)^2}, \tag{1}$$

where N_c and N_s are two constants, and

$$d_s = \|p_1 - p_2\|_2 = \sqrt{(u_1 - u_2)^2 + (v_1 - v_2)^2}$$

$$d_c = \|\mathbf{c}(p_1) - \mathbf{c}(p_2)\|_2 = \sqrt{(l(p_1) - l(p_2))^2 + (a(p_1) - a(p_2))^2 + (b(p_1) - b(p_2))^2}.$$

Given a set $\{s_i\}_{i=1}^K$ of evenly distributed seeds in the image I, SLIC partitions I using Voronoi diagram $\{\mathcal{V}(s_i)\}_{i=1}^K$ and then iteratively improves the Voronoi cells by moving the seeds to their centers of mass, resulting the so-called *centroidal Voronoi tessellation*.

Mathematically speaking, a CVT is defined as follows: Let $\rho : I \to \mathbb{R}^+$ be a density function defined on I. For a Voronoi cell $\mathcal{V}(s_i)$, its center of mass c_i is

$$c_i = \frac{\int_{x \in \mathcal{V}(s_i)} x\rho(x)dx}{\int_{x \in \mathcal{V}(s_i)} \rho(x)dx}. \tag{2}$$

The Voronoi tessellation $\{\mathcal{V}(s_i)\}_{i=1}^K$ is a CVT if, for each Voronoi cell, the center of mass coincides with the seed, i.e., $c_i = s_i$, $1 \le i \le K$. Du et al. [2] showed that a CVT is the minimizer of the following energy E

$$E\left(\{s_i\}_{i=1}^K, \{\mathcal{V}(s_i)\}_{i=1}^K\right) = \sum_{i=1}^K \int_{x \in \mathcal{V}(s_i)} \rho(x) d(x, s_i) dx, \tag{3}$$

where $d(x, y)$ measures the distance between x and y. They also showed that the solution always exists.

SLIC sets the distance $d(x, g_i) = D(x, g_i)$, as defined in Eqn. (1), and computes CVT using the Lloyd method, which iteratively moves each seed to the corresponding center of mass. We outline SLIC in Algorithm 1. SLIC adopts two heuristic strategies: First, rather than explicitly constructing the Voronoi cells, for each seed s_i, it computes distances from s_i to the pixels within a $2S \times 2S$ window centered at s_i (lines 6-13) and then assigns a pixel to the seed with the least distance. This local search also distinguishes SLIC from the conventional K-means method, which has to compute the distances between s_i and *every* pixel in the image. Second, it does not compute the center of mass using the area integral in Eqn. (2). Instead, it finds the centroid c_i as the mean vector of all the pixels belonging to the Voronoi cell (line 16). Computational results show that SLIC converges in only 10 iterations for real-world images [1]. As a result, SLIC has an $O(N)$ time complexity, which is independent of the number of superpixels K. In contrast, the conventional K-means method runs in $O(KNN_{iter})$, where N_{iter} is the number of iterations.

Algorithm 1 SLIC [1]

```
Input: An image $I$ of $N$ pixels, the desired number of superpixels $K$, the maximal number of iterations $iter_{max}$ and the convergence threshold $\varepsilon$.
Output: $K$ superpixels of similar sizes.
 1: Initialize seeds $\{s_i\}_{i=1}^{K}$ at regular grids with step length $S = \sqrt{N/K}$.
 2: Move each seed to the lowest gradient position in a $3\times 3$ neighborhood.
 3: Initialize label $l(p) = -1$ and distance $d(p) = \infty$ for each pixel $p$.
 4: Initialize the residual error $err = \infty$ and $iter = 0$.
 5: while $err > \varepsilon$ and $iter \le iter_{max}$ do
 6:   for each seed $s_i$ do
 7:     for each pixel $p$ in a $2S \times 2S$ region around $s_i$ do
 8:       Compute the distance $D = D(s_i, p)$ between $s_i$ and $p$.
 9:       if $D < d(p)$ then
10:         $d(p) = D; l(p) = i$.
11:       end if
12:     end for
13:   end for
14:   $err = 0$.
15:   for each seed $s_i$ do
16:     Compute average $c_i$ of pixels in the cluster of $s_i$.
17:     $err$ += $\|c_i - s_i\|^2$.
18:     $s_i = c_i$.
19:   end for
20:   $iter$ ++.
21: end while
```

2.2. SSS

SLIC is conceptually simple and highly efficient. However, due to the constant CVT density function $\rho(x) \equiv 1, \forall x \in I$, it produces uniform superpixels, i.e., superpixels have similar sizes everywhere. Since many real-world images may contain complicated contents, it is highly desired to develop content-sensitive superpixels, i.e., small superpixels in content-dense regions and large superpixels in content-sparse regions. Wang et al. [18] computed content-sensitive superpixels using a geometric flow [9] into the CVT optimization framework. In contrast to SLIC that uses Euclidean distances, SSS adopts geodesic distances defined as follows:

$$d(p_1, p_2) = \min_{P_{p_1,p_2}} \int_0^1 D(P_{p_1,p_2}(t)) \|\dot{P}_{p_1,p_2}(t)\| dt \quad (4)$$

where $P_{p_1,p_2}(t)$ is a parameterized path connecting pixels p_1 ($t = 0$) and p_2 ($t = 1$). The weight function $D(z)$ penalizes image boundaries [9],

$$D(z) = e^{\frac{edge(z)}{\upsilon}}, \;\; edge(z) = \frac{\|\nabla I\|}{G_\sigma * \|\nabla I\| + \gamma} \quad (5)$$

where υ is a scaling parameter, $edge(z)$ is a normalized edge measurement, G_σ is the Gaussian functions with the standard deviation σ, and γ is a small constant to alleviate the affect of weak intensity boundary.

Compared with Euclidean distances in Eqn. (1), geodesic distances in Eqn. (4) penalize image boundary, hereby are an effective measure of content-sensitivity. Computational results show that Wang et al.'s method [18] can compute high-quality content-sensitive superpixels that exhibit high boundary adherence. However, since it is computationally expensive to measure geodesic distances, their method is among the slowest algorithms in our experiments.

3. Overview

Manifold SLIC extends SLIC to compute content-sensitive superpixels, meanwhile it inherits all the favorable features of SLIC, such as simplicity and high performance.

Similar to SLIC [1], we represent the color in the CIELAB color space and denote by $\mathbf{c}(u,v) = (l(u,v), a(u,v), b(u,v))$ the color at the pixel (u,v) in the image I. Then we define a stretching map $\Phi : I \to \mathbb{R}^5$ to send pixels to a 2-manifold $\mathcal{M}$ embedded in the 5-dimensional combined image and color space,

$$\Phi(u,v) = (\lambda_1 p, \lambda_2 \mathbf{c}) = (\lambda_1 u, \lambda_1 v, \lambda_2 l, \lambda_2 a, \lambda_2 b), \quad (6)$$

where λ_1 and λ_2 are global stretching factors. We set $\lambda_1 = \frac{1}{N_s}$ and $\lambda_2 = \frac{1}{N_c}$ and adopt the SLIC metric D in Eqn. (1) to measure the distance between points on manifold $\mathcal{M}$, i.e.,

$$D(\Phi(p_1), \Phi(p_2)) = \sqrt{\lambda_1^2 d_s^2 + \lambda_2^2 d_c^2}. \quad (7)$$

For a pixel $p = (u,v)$, we denote by $\square_p$ the unit square 1×1 centered at p. Let p_1, p_2, p_3, p_4 be the four corners of

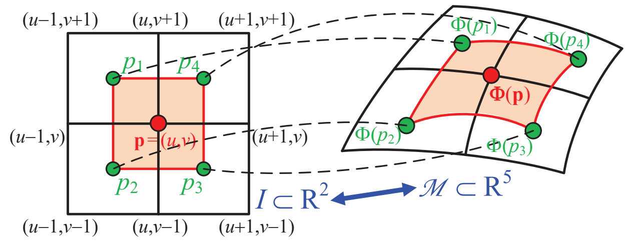

Figure 2. Measuring area on the 2-manifold $\mathcal{M}$ embedded in $\mathbb{R}^5$.

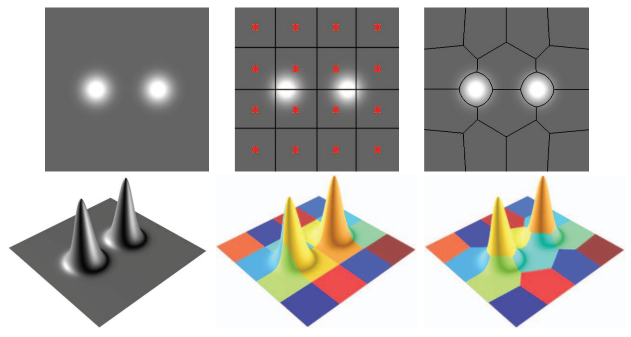

Figure 3. Overview of manifold SLIC on a synthetic greyscale image I. We represent I as a 2-manifold embedded in $\mathbb{R}^3$, denoted by $\mathcal{M} = \Phi(u, v) \subset \mathbb{R}^3$, whose area elements are a good measure of the content density in I (see (a)). Initially, we distribute $K(= 16)$ seeds $\{s_i\}_{i=1}^K$ uniformly in I, leading to a Voronoi diagram on $\mathcal{M}$ (see (b)). We then improve the Voronoi diagram by computing restricted centroidal Voronoi tessellation (RCVT) $\{\mathcal{V}(\Phi(s_i))\}_{i=1}^K$on $\mathcal{M}$ — a uniform tessellation on $\mathcal{M}$ where the Voronoi cells are of similar sizes. Finally, the RCVT induces the content-sensitive superpixels $\{\Phi^{-1}(\mathcal{V}(\Phi(s_i)))\}_{i=1}^K$ in the image domain (see (c)).

$\square_p$, each of which is determined by the average of the four neighboring pixels. The square $\square_p$ consists of two triangles, i.e., $\square_p = \triangle p_1p_2p_3 \bigcup \triangle p_3p_4p_1$. Then we approximate the area of the *curved* triangle $\Phi(\triangle p_1p_2p_3)$ by the area of *planar* triangle $\triangle\Phi(p_1)\Phi(p_2)\Phi(p_3)$,

$$Area(\Phi(\triangle p_1p_2p_3)) \approx \frac{1}{2}\|\overrightarrow{\Phi(p_2)\Phi(p_1)}\|\|\overrightarrow{\Phi(p_2)\Phi(p_3)}\| \sin\theta, \tag{8}$$

where θ is the angle between vectors $\overrightarrow{\Phi(p_2)\Phi(p_1)}$ and $\overrightarrow{\Phi(p_2)\Phi(p_3)}$. Note that the length $\|\overrightarrow{\Phi(x)\Phi(y)}\|$ is measured using the metric D in Eqn. (7). $Area(\Phi(\triangle p_3p_4p_1)$ can be computed in a similar way. See Figure 2. The area of a region $\Phi(\Omega) \subset \mathcal{M}$ is simply the sum of $Area(\Phi(\square_{p_i}))$ for all pixels $p_i \in \Omega$.

Our method is based on an important observation: for a region $\Omega \subset I \subset \mathbb{R}^2$, the area of the corresponding region $\Phi(\Omega) \subset M$ on $\mathcal{M}$ depends on both the area of Ω and the intensity or color variation in Ω. The higher the variation of colors in Ω, the larger the area of $\Phi(\Omega)$, and vice versa. If we can compute a *uniform* tessellation on $\mathcal{M}$, the inverse mapping Φ^{-1} will induce the *content-sensitive* tessellation on I. See Figure 3. Towards this goal, we propose two simple yet effective techniques: computing restricted CVT (Section 4) and locally updating bad-shaped Voronoi cells (Section 5). We also outline the manifold SLIC in Algorithm 2 and highlight its differences to SLIC in blue.

Algorithm 2 Manifold SLIC

```
Input: An image $I$ of $N$ pixels, the desired number of superpixels $K$, the maximal number of iterations $iter_{max}$ and the convergence threshold $\varepsilon$.
Output: $K$ content-sensitive superpixels.
1: Initialize seeds $\{s_i\}_{i=1}^K$ at regular grids with step length $S = \sqrt{N/K}$.
2: Move each seed to the lowest gradient position in a $3\times3$ neighborhood.
3: Initialize label $l(p) = -1$ and distance $d(p) = \infty$ for each pixel $p$.
4: Initialize the residual error $err = \infty$ and $iter = 0$.
5: Compute $Area(\Phi(\square_p))$ for each pixel $p \in I$.
6: Compute a local search range $\Xi = \frac{4\sum_{i=1}^K Area(\Phi(\square_{p_i}))}{K}$.
7: while $err > \varepsilon$ and $iter \le iter_{max}$ do
8:     for each seed $s_i$ do
9:         Compute $Area(\Phi(\Omega(s_i)))$ of a $2S \times 2S$ region $\Omega(s_i)$ centered at $s_i$.
10:        Compute a scaling factor $\lambda_i = \sqrt{\frac{\Xi}{Area(\Phi(\Omega(s_i)))}}$.
11:        if $iter > 0$ and $\lambda_i < \tau$ and $Area(\mathcal{V}_{\mathcal{M}}(\Phi(s_i))) > \Xi/4$ then
12:            Split Voronoi cell $\mathcal{V}_{\mathcal{M}}(\Phi(s_i))$. (Section 5.1)
13:        end if
14:    end for
15:    Merge the Voronoi cells whose areas are small and whose seeds are close to each other. (Section 5.2)
16:    for each seed $s_i$ do
17:        for each pixel $p$ in a $2\lambda_i S \times 2\lambda_i S$ region centered at $s_i$ do
18:            Compute the distance $D = D(\Phi(s_i), \Phi(p))$ using Eqn. (7).
19:            if $D < d(p)$ then
20:                $d(p) = D$; $l(p) = i$.
21:            end if
22:        end for
23:    end for
24:    $err = 0$.
25:    for each seed $s_i$ do
26:        Compute $Area(\mathcal{V}_{\mathcal{M}}(\Phi(s_i)))$.
27:        Compute the mass center $m_i$ of $\mathcal{V}_{\mathcal{M}}(\Phi(s_i))$ using Eqn. (11) and set $c_i = P(m_i)$ using Eqn. (19).
28:        $err$ += $\|c_i - s_i\|^2$.
29:        $s_i = c_i$.
30:    end for
31:    $iter$ ++.
32: end while
```

4. Computing Restricted CVT

The quality of CVT plays a critical role in the content-sensitive superpixels. Since it is expensive to compute *exact* CVTs on curved manifolds [11, 12, 20], we compute the *restricted* centroidal Voronoi tessellation (RCVT), which approximates the exact CVT well for K in a proper range, e.g., $K > 200$ in images of resolution 512×512.

4.1. Restricted Voronoi Diagram and RCVT

Let $S = \{s_i | s_i \in I, 1 \le i \le K\}$ be the set of seeds in the image I and $G = \{\Phi(s_i)\}_{i=1}^K$ the corresponding generators on the manifold $\mathcal{M}$. The *Euclidean* Voronoi cell of a generator $\Phi(s_i)$, denoted by $\mathcal{V}_{\mathbb{R}^5}$, is

$$\begin{aligned}\mathcal{V}_{\mathbb{R}^5}(\Phi(s_i)) = \{x \in \mathbb{R}^5 | \|x - \Phi(s_i)\|_2 \le \\ \|x - \Phi(s_j)\|_2, \forall j \ne i, \Phi(s_j) \in G\}.\end{aligned} \tag{9}$$

Restricting $\mathcal{V}_{\mathbb{R}^5}$ to the manifold $\mathcal{M}$, we obtain the *restricted* Voronoi cell $\mathcal{V}_{\mathcal{M}}(\Phi(s_i)) \triangleq \mathcal{M} \bigcap \mathcal{V}_{\mathbb{R}^5}(\Phi(s_i))$. The restricted Voronoi diagram $RVD(G, \mathcal{M})$ [4] is the collection of restricted Voronoi cells satisfying

$$RVD(G, \mathcal{M}) = \{\mathcal{V}_{\mathcal{M}}(\Phi(s_i)) \ne \emptyset | \forall \Phi(s_i) \in G\} \tag{10}$$

Edelsbrunner and Shah [4] showed that $RVD(G, \mathcal{M})$ is a finite closed covering of $\mathcal{M}$. For a restricted Voronoi cell $\mathcal{V}_{\mathcal{M}}(\Phi(s_i))$, its mass centroid m_i is

$$m_i = \frac{\int_{r \in \mathcal{V}_{\mathcal{M}}(\Phi(s_i))} r dr}{\int_{r \in \mathcal{V}_{\mathcal{M}}(\Phi(s_i))} 1 dr} \tag{11}$$

Then we define restricted CVT as follows:

Definition 1. *Let $X = \{x_i | x_i \in \mathbb{R}^n, 1 \le i \le K\}$ be a set of points in $\mathbb{R}^n$ and $\mathcal{M}$ be a 2-manifold embedded in $\mathbb{R}^n$. A restricted Voronoi diagram $RVD(X, \mathcal{M})$ is a restricted CVT (or RCVT) if each generator $x_i \in X$ is the mass centroid of its restricted Voronoi cell.*

Theorem 1. *Let $\mathcal{M}$ be a 2-manifold embedded in $\mathbb{R}^n$ and $K \in \mathbb{Z}_+$ a positive integer. For an arbitrary set X of points $\{x_i\}_{i=1}^K$ in $\mathbb{R}^n$ and an arbitrary tessellation $\{V_i\}_{i=1}^K$ on $\mathcal{M}$, $\bigcup_{i=1}^K V_i = \mathcal{M}$, $V_i \bigcap V_j = \emptyset$, $\forall i \ne j$, define the CVT energy functional as follows:*

$$\mathcal{E}(\{(x_i, V_i)\}_{i=1}^K) = \sum_{i=1}^K \int_{r \in V_i} d^2(r, x_i) dr \tag{12}$$

Then the necessary condition for $\mathcal{E}$ being minimized is that $\{(x_i, V_i)\}_{i=1}^K$ is a RCVT of $\mathcal{M}$.

Proof. The proof consists of two parts: (1) if $\{V_i\}_{i=1}^K$ is fixed, then minimization of $\mathcal{E}$ requires that each x_i is the mass centroid of V_i; and (2) if $\{x_i\}_{i=1}^K$ is fixed, then minimization of $\mathcal{E}$ requires that $\{V_i\}_{i=1}^K$ is $RVD(\{x_i\}_{i=1}^K, \mathcal{M})$.

First, examining the first variation of $\mathcal{E}$ with respect to a single point, say x_i, we have

$$\mathcal{E}(x_i + \epsilon v) - \mathcal{E}(x_i) = \int_{r \in V_i} \{d^2(r, x_i + \epsilon v) - d^2(r, x_i)\} dr \tag{13}$$

where $v \in \mathbb{R}^n$ and $\epsilon \in \mathbb{R}$ are arbitrary. Note that in Eqn. (13), the fixed variables in the argument of $\mathcal{E}$ are not listed. Dividing the left hand side by ϵ and taking $\epsilon \to 0$, we have

$$x_i = \frac{\int_{r \in V_i} r dr}{\int_{r \in V_i} 1 dr} \tag{14}$$

implying that x_i is the mass centroid of the region V_i.

Second, we fix the points in X and choose a tessellation $\{V_i\}_{i=1}^K$ other than the restricted Voronoi tessellation $\{RVD(\{x_i\}_{i=1}^K, \mathcal{M})\}$. Then we compare $\mathcal{E}(\{(x_i, \mathcal{V}_{\mathcal{M}}(x_i))\}_{i=1}^K)$ with $\mathcal{E}(\{(x_i, V_i)\}_{i=1}^K)$. For any point $r \in \mathcal{M}$ belonging to a restricted Voronoi cell $\mathcal{V}_{\mathcal{M}}(x_i)$, we have

$$d(r, x_i) \le d(r, x_j), \; x_j \in X \tag{15}$$

Since $\{V_i\}_{i=1}^K$ is not a Voronoi tessellation, the inequality (15) must hold strictly over some measure nonzero set in $\mathcal{M}$. Accordingly,

$$\mathcal{E}(\{(x_i, \mathcal{V}_{\mathcal{M}}(x_i))\}_{i=1}^K) < \mathcal{E}(\{(x_i, V_i)\}_{i=1}^K) \tag{16}$$

Thus $\mathcal{E}$ is minimized when $\{V_i\}_{i=1}^K$ are chosen to be $\{\mathcal{V}_{\mathcal{M}}(x_i)\}_{i=1}^K$. □

Given the initial generators $\{x_i\}_{i=1}^K$, $x_i \in \mathcal{M}$, manifold SLIC adopts the Lloyd-like method to iteratively compute RCVT (lines 7-32 in Algorithm 2). Lines 8-14 check if there are bad-shaped Voronoi cells. If so, split these cells. Line 15 checks those Voronoi cells with small areas. If the generators of two neighboring Voronoi cells are close to each other, we merge them into a single Voronoi cell. Lines 16-23 compute the restricted Voronoi tessellation $RVD(X, \mathcal{M})$. Lines 25-30 move the generator of each restricted Voronoi cell to its mass center. The algorithm terminates when the generators s_i do not move or the iteration number reaches a user-specified threshold.

Denote by X_i the set $\{x_i\}_{i=1}^K$ at each iteration i in Algorithm 2. The Lloyd algorithm is a fixed point iteration of a Lloyd map $\mathbf{T}$:

$$X_n = \mathbf{T}(X_{n-1}), \;\text{ for } n \ge 1 \tag{17}$$

The convergence of the Lloyd algorithm directly obtained from the proof of Theorem 1:

$$\begin{aligned}&\mathcal{E}(X_{n+1}, RVD(X_{n+1}, \mathcal{M})) \le \mathcal{E}(X_{n+1}, RVD(X_n, \mathcal{M})) \\ &\le \mathcal{E}(X_n, RVD(X_n, \mathcal{M}))\end{aligned} \tag{18}$$

The difference between the proposed RCVT and the constrained CVT (CCVT) [3] is that the center of mass of a Voronoi cell in CCVT is always on the manifold $\mathcal{M}$, whereas RCVT does not have such a requirement. This seemingly minor change is indeed critical to improve the runtime performance significantly.

4.2. A Simple Yet Efficient Method

The bottleneck of the Lloyd method is to form the Voronoi diagram $RVD(G, \mathcal{M})$ for the set of seeds $G = \{\Phi(s_i)\}_{i=1}^{K}$. Inspired by the local search in SLIC, we develop a *local* method to approximate $RVD(G, \mathcal{M})$ in $O(N)$ time.

Observe that RCVT tends to generate uniform restricted Voronoi cells (RVC) on $\mathcal{M}$. Therefore, the area of each RVC is roughly $\frac{Area(\mathcal{M})}{K}$. To speed up the construction of a RVC, we limit the size of searching area for each generator to be $\frac{4Area(\mathcal{M})}{K}$. To quickly find the limited search areas, for each RVC on $\mathcal{M}$, we project its mass centroid back to the image plane by

$$P(m) = (u, v), \tag{19}$$

where $m = (u, v, \frac{\lambda_2}{\lambda_1}l, \frac{\lambda_2}{\lambda_1}a, \frac{\lambda_2}{\lambda_1}b) \in \mathbb{R}^5$. We use a $2S \times 2S$ region Ω centered at $P(m)$ in the image I as the initial guess, where $S = \sqrt{N/K}$. Then we adjust the local region Ω by calculating an adaptive scaling factor $\lambda = \sqrt{\Xi/Area(\Phi(\Omega))}$. Finally we approximate the limited searching area by the set $\{\Phi(p) | p \in \Omega' \subset I\}$, where Ω' is the $2\lambda S \times 2\lambda S$ region centered at $P(m)$ in image I.

Now we show that Algorithm 2 runs in $O(N)$ time, which is independent of the number of superpixels K. The key is to show λ_i is bounded by a constant $c_{\max} = \max\{Area(\Phi(\square_{p_j})), p_j \in I\}$ that is determined by the color variation of the image I. To see this, note that λ_i reaches maximum when $Area(\Phi(\Omega(s_i)))$ is minimum. $Area(\Phi(\Omega(s_i)))$ is minimum when $\Phi(\Omega(s_i))$ is flat (having the same color), i.e., $Area(\Phi(\Omega(s_i))) = 4S^2 = 4N/K$. Therefore $\lambda_i = \sqrt{\Xi/Area(\Phi(\Omega(s_i)))} \leq \sqrt{Area(\mathcal{M})/N} \leq \sqrt{c_{\max}}$.

In each local search region, there are at most $2\lambda_i S \times 2\lambda_i S \leq 4c_{\max}N/K$ pixels. Then the total number of pixels visited in all K local regions is bounded by $4c_{\max}N$. Therefore, Algorithm 2 takes linear time $O(N)$.

5. Locally Updating Voronoi Cells

5.1. The Splitting Operator

The splitting operator is used to produce more seeds in content-rich regions. In line 12 of Algorithm 2, a seed s_i is replaced by four new seeds if the following conditions hold:

- The local search region $\Omega' = 2\lambda_i S \times 2\lambda_i S$ around s_i contains very rich content information. This condition is determined by $Area(\Phi(\Omega'(s_i)))$ in $\mathcal{M}$. If it is sufficiently large, i.e., the adaptive scaling factor $\lambda_i = \sqrt{\Xi/Area(\Phi(\Omega'(s_i)))}$ is less than a small threshold ($\tau = 0.5$ in Algorithm 2), we consider that this condition holds.

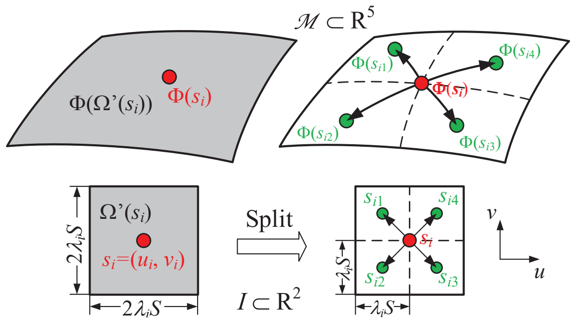

Figure 4. Illustration of the splitting operator. $\Omega'(s_i)$ is a $2\lambda_i S \times 2\lambda_i S$ region on the image I around s_i. If $Area(\Phi(\Omega'(s_i))) > 4\Xi$ (i.e., $\lambda_i < 0.5$), where $\Xi = 4Area(\mathcal{M})/K$ is a fixed area of a local search region in image manifold $\mathcal{M}$, the splitting operator replaces $s_i = (u_i, v_i)$ into four new generators $s_{i1} = (u_i - \frac{\lambda_i S}{2}, v_i + \frac{\lambda_i S}{2})$, $s_{i2} = (u_i - \frac{\lambda_i S}{2}, v_i - \frac{\lambda_i S}{2})$, $s_{i3} = (u_i + \frac{\lambda_i S}{2}, v_i - \frac{\lambda_i S}{2})$ and $s_{i4} = (u_i + \frac{\lambda_i S}{2}, v_i + \frac{\lambda_i S}{2})$. We set the adaptive scaling factors as $\lambda_{i1} = \lambda_{i2} = \lambda_{i3} = \lambda_{i4} = \lambda_i/2$.

- To prevent endless loop, we can only split a Voronoi cell whose area is larger than $\Xi/4$.

If s_i is the to-be-split seed, we partition the local adaptive local search region $\Omega' = 2\lambda_i S \times 2\lambda_i S$ into four identical sub-regions and generate four new seeds at the centers of sub-regions. For each new seed, we assign the adaptive scaling factor to be $\lambda_i/2$. Due to this regular 1-4 splitting strategy, we set the threshold $\tau = 0.5$ in Algorithm 2 ($\tau = 0.5$ means that $Area(\Phi(\Omega(s_i)))$ is four times larger than the area Ξ and after splitting, the expected area of each subregion is still no less than Ξ). See Figure 4. The positions of the new seeds and their associated adaptive scaling factors will be further optimized in the next iteration.

5.2. The Merging Operator

The splitting operator produces more seeds than the user specified number K. To meet the user's requirement, Algorithm 2 adopts the merging operator to reduce the number of seeds in content-sparse regions.

We consider the following two cases. First, if the area of $\mathcal{V}_{\mathcal{M}}(\Phi(s_i))$ of a seed is very small ($Area(\mathcal{V}_{\mathcal{M}}(\Phi(s_i))) < Area(\mathcal{M})/8K$ in our experiment), we randomly choose a neighbor seed s_j and merge s_i and s_j. Second, if the sum of areas $Area(\mathcal{V}_{\mathcal{M}}(\Phi(s_i))) + Area(\mathcal{V}_{\mathcal{M}}(\Phi(s_j)))$ of two neighbor seeds s_i and s_j is smaller than a threshold τ_{area}, they are merged into one. We choose the value of τ_{area} to prevent the merged seed being split again by the splitting operator. Denote by s_k the merged seed of s_i and s_j and let $Area(\widetilde{\mathcal{V}}_{\mathcal{M}}(\Phi(s_k))) = Area(\mathcal{V}_{\mathcal{M}}(\Phi(s_i))) +$

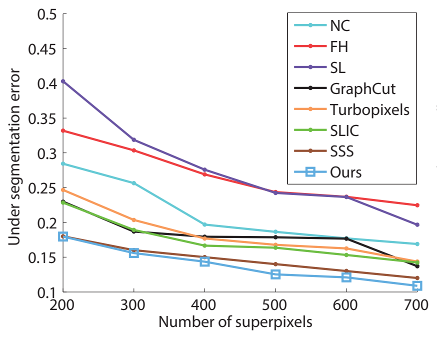

(a) Under segmentation error

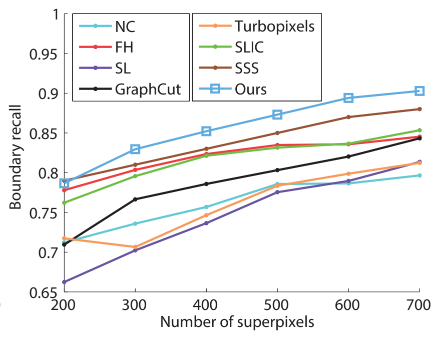

(b) Boundary recall

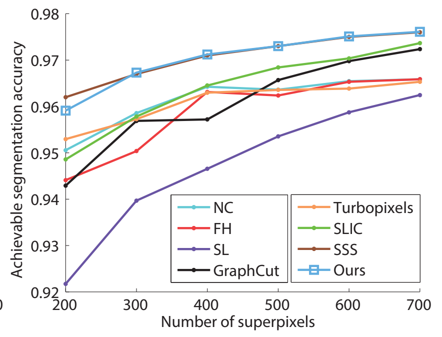

(c) Achievable segmentation accuracy (ASA)

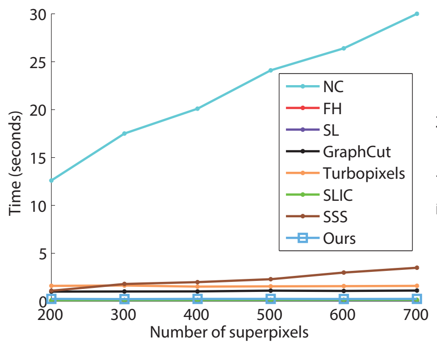

(d) Runtime with respective to K

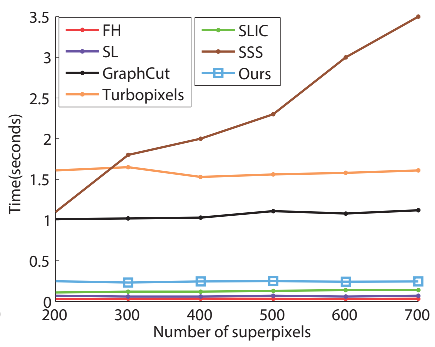

(e) Runtime in (d) without NC

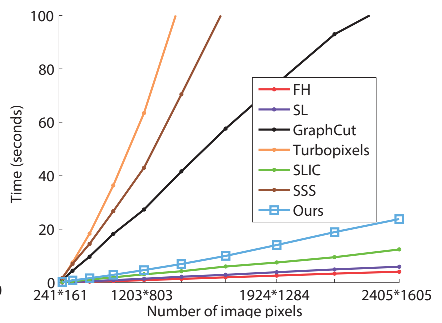

(f) Runtime with respective to N

Figure 5. Evaluation of representative algorithms and manifold SLIC on the BSDS500 benchmark for $K \in [200, 700]$. Superpixels produced by manifold SLIC have the least under segmentation error and the highest boundary recall ratio, indicating that our method adheres to image boundaries very well. Both SSS and manifold SLIC lead to similar ASA, however, our method significantly outperforms SSS in terms of runtime performance.

$Area(\mathcal{V}_{\mathcal{M}}(\Phi(s_j)))$. We use $Area(\widetilde{\mathcal{V}}_{\mathcal{M}}(\Phi(s_k)))$ as a low-cost approximation of $Area(\mathcal{V}_{\mathcal{M}}(\Phi(s_k)))$. We choose $\tau_{area} = \Xi/5$, i.e., $Area(\widetilde{\mathcal{V}}_{\mathcal{M}}(\Phi(s_k))) < \Xi/5$, where $\Xi/5$ characterizes content-sparse areas by noting that in Algorithm 2, a seed s_i is split only if $Area(\mathcal{V}_{\mathcal{M}}(\Phi(s_i))) > \Xi/4$.

After merging two neighboring seeds s_i and s_j, we compute the position of the new seed s_k as

$$s_k = P(\widetilde{g}_k), \tag{20}$$

where P is the projection operator defined in Eqn. (19) and

$$\widetilde{g}_k = \frac{\Phi(s_i) \cdot Area(\mathcal{V}_{\mathcal{M}}(\Phi(s_i))) + \Phi(s_j) \cdot Area(\mathcal{V}_{\mathcal{M}}(\Phi(s_j)))}{Area(\mathcal{V}_{\mathcal{M}}(\Phi(s_i))) + Area(\mathcal{V}_{\mathcal{M}}(\Phi(s_j)))} \tag{21}$$

We show the pseudo codes of the *splitting* and *merging* operators and an illustrative example in the supplementary material.

6. Experimental Results

We implemented manifold SLIC in C++ and tested it on a PC with an Intel I7-860 CPU (2.80GHz) and 8GB RAM. We compared manifold SLIC with several representative methods, including NC [16], FH [5], SL [15], GraphCut [17], Turbopixels [9], SLIC [1] and SSS [18], on the BSDS500 benchmark [13], where each image has a ground truth segmentation. Following [18], we evaluated the algorithms on 200 randomly selected images of resolution 481×321.

Adherence to Boundaries. As dense over-segmentation of images, superpixels should well preserve the boundary of ground-truth segmentations. Under segmentation error and boundary recall are the standard measures for boundary adherence [9, 1, 18]. The former measures the tightness of superpixels that overlap with a ground-truth segmentation, and the latter measures what fraction of the ground truth edges fall within at least two pixels of a superpixel boundary. A high boundary recall means that very few true edges are missed. As shown in Figure 5(a) and (b), superpixels generated by manifold SLIC have the least under segmentation error and the highest boundary recall ratio, demonstrating its ability to adhere to image boundaries.

Content Sensitivity. The supplementary material shows typical results of manifold SLIC, in which one can clearly see that the computed superpixels are content sensitive, i.e., they are small in content dense regions and large in content sparse regions. The content sensitive feature is due to the fact that regions of high color variance have larger areas on $\mathcal{M}$.

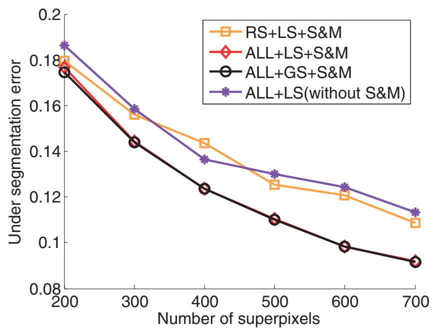

(a) Under segmentation error

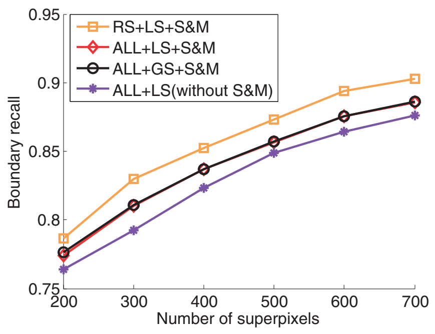

(b) Boundary recall

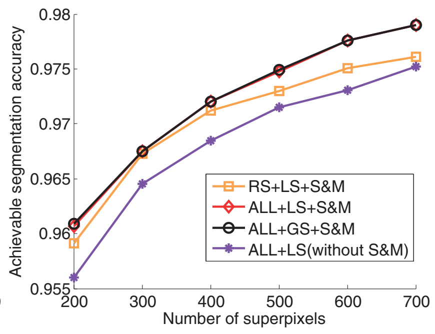

(c) Achievable segmentation accuracy (ASA)

Figure 6. Evaluation of various combinations in the setting of Manifold SLIC on the BSDS500 benchmark for $K \in [200, 700]$. Notations: random subset in BSDS (RS); all the images in BSDS (ALL); local search proposed in Section 4.2 (LS); global search on the entire manifold (GS); with the splitting and merging operators (S&M); without the splitting and merging operators (without S&M).

Achievable Segmentation Accuracy (ASA). Superpixels can be used as a preprocessing step for the subsequent segmentation algorithms. ASA, defined as the highest accuracy in all possible segmentations that use superpixels as input, is the upper bound of accuracy of a segmentation [18]. In general, the more number of superpixels, the better ASA one can obtain. As Figure 5(c) shows, the ASA plot of superpixels produced by manifold SLIC is comparable to that of SSS for $K \geq 300$.

Runtime Performance. Similar to SLIC, manifold SLIC has an $O(N)$ time complexity, which is independent of the number of superpixels K. Figure 5(d) plots the runtime curves for all testing methods. We observe that FH, SLIC, SL and manifold SLIC are among the fastest algorithms. Our method significantly outperforms SSS in terms of runtime performance. For example, manifold SLIC runs 10 times faster than SSS for $K \in [400, 700]$.

Experiments on the Entire BSDS500 Dataset. Compared with randomly selected images (RS+LS+S&M vs. ALL+LS+S&M), we observe the improvement of under segmentation error and achievable segmentation accuracy. However, the performance of boundary recall drops slightly. See Figure 6.

Effect on the Local Search. We propose a local method in Section 4.2 to approximate $RVD(G, \mathcal{M})$ in $O(N)$ time. In Figure 6, we compare the approximate solution of our local method and the exact solution obtained by searching on the entire manifold (compare ALL+LS+S&M with ALL+GS+S&M). Judging the results on three metrics, we observe almost no difference between the exact solution and the approximate one.

Roles of the Splitting and Merging Operators. Our method computes restricted CVT on a 2-manifold $\mathcal{M} \subset \mathbb{R}^5$. The motivation is to compute superpixels with similar areas on $\mathcal{M}$. The splitting operator adds more seeds in cells of large areas and the merging operator reduces the seeds in cells of small areas. Without these two operators, Algorithm 2 reduces to a simple Lloyd algorithm which converges only to a local minimum. Figure 6 compares the performance of Algorithm 2 with and without these two operators (ALL+LS+S&M vs, ALL+LS(without S&M)) using three metrics. The results demonstrate that the two operators play an important role to jump out of the local minimum, leading to a good approximation of the global minimization to the CVT energy defined in Eqn. (12). It is also worth noting that the splitting and merging operators are designed for our manifold setting and cannot be used in SLIC, because starting from initial seeds, superpixels in each iteration in SLIC have similar areas in the image plane.

7. Conclusion

Manifold SLIC extends the conventional SLIC method to compute content-sensitive superpixels. It maps the input image I to a 2-dimensional manifold $\mathcal{M}$ embedded in the combined image and color space $\mathbb{R}^5$, whose area elements reflect the density of image content. We propose a simple yet efficient method to compute restricted CVT on $\mathcal{M}$, which induces the content-sensitive superpixels in I. Computational results on the Berkeley benchmark show that our method outperforms the existing superpixel methods in terms of under segmentation error, boundary recall and achievable segmentation accuracy. Manifold SLIC is also 10 times faster than the state-of-the-art content-sensitive superpixel algorithm. Our future work is to apply GPU parallel computing [7] to further improve the performance of manifold SLIC for high-resolution images.

Acknowledgment

This work was supported by Royal Society-Newton Advanced Fellowship, the Natural Science Foundation of China (61521002, 61432003, 61322206), TNList Foundation, Tsinghua University Initiative Scientific Research Program, RG23/15 and MOE2013-T2-2-011.

References

[1] R. Achanta, A. Shaji, K. Smith, A. Lucchi, P. Fua, and S. Süsstrunk. SLIC superpixels compared to state-of-the-art superpixel methods. *IEEE Trans. Pattern Analysis and Machine Intelligence*, 34(11):2012–2281, 2012.

[2] Q. Du, V. Faber, and M. Gunzburger. Centroidal Voronoi tessellations: Applications and algorithms. *SIAM Review*, 41(4):637676, 1999.

[3] Q. Du, M. D. Gunzburger, and L. Ju. Constrained centroidal voronoi tessellations for surfaces. *SIAM Journal on Scientific Computing*, 24(5):1488–1506, 2003.

[4] H. Edelsbrunner and N. R. Shah. Triangulating topological spaces. *International Journal of Computational Geometry & Applications*, 7(4):365–378, 1997.

[5] P. F. Felzenszwalb and D. P. Huttenlocher. Efficient graph-based image segmentation. *International Journal of Computer Vision*, 59(2):167–181, 2004.

[6] B. Fulkerson, A. Vedaldi, and S. Soatto. Class segmentation and object localization with superpixel neighborhoods. In *IEEE International Conference on Computer Vision (ICCV '09)*, pages 670–677, 2009.

[7] Y.-S. Leung, X. Wang, Y. He, Y.-J. Liu, and C. Wang. A unified framework for isotropic meshing based on narrow-banded euclidean distance transformation. *Computational Visual Media*, 1(3):239–251, 2015.

[8] A. Levinshtein, C. Sminchisescu, and S. Dickinson. Optimal contour closure by superpixel grouping. In *Europeon Conference on Computer Vision (ECCV '10)*, pages 480–493, 2010.

[9] A. Levinshtein, A. Stere, K. N. Kutulakos, D. J. Fleet, S. J. Dickinson, and K. Siddiqi. Turbopixels: Fast superpixels using geometric flows. *IEEE Trans. Pattern Analysis and Machine Intelligence*, 31(12):2290–2297, 2009.

[10] M.-Y. Liu, O. Tuzel, S. Ramalingam, and R. Chellappa. Entropy rate superpixel segmentation. In *IEEE Conference on Computer Vision and Pattern Recognition (CVPR '11)*, pages 2097–2104, 2011.

[11] Y.-J. Liu. Semi-continuity of skeletons in 2-manifold and discrete Voronoi approximation. *IEEE Trans. Pattern Analysis and Machine Intelligence*, 37(9):1938–1944, 2015.

[12] Y.-J. Liu, Z.-Q. Chen, and K. Tang. Construction of iso-contours, bisectors and Voronoi diagrams on triangulated surfaces. *IEEE Trans. Pattern Analysis and Machine Intelligence*, 33(8):1502–1517, 2011.

[13] D. Martin, C. Fowlkes, D. Tal, and J. Malik. A database of human segmented natural images and its application to evaluating segmentation algorithms and measuring ecological statistics. In *Proc. 8th Int'l Conf. Computer Vision*, volume 2, pages 416–423, July 2001.

[14] B. Mičušík and J. Košecká. Multi-view superpixel stereo in urban environments. *International Journal of Computer Vision*, 89(1):106–119, 2010.

[15] A. P. Moore, S. J. D. Prince, J. Warrell, U. Mohammed, and G. Jones. Superpixel lattices. In *IEEE Conference on Computer Vision and Pattern Recognition (CVPR '08)*, pages 1–8, 2008.

[16] J. Shi and J. Malik. Normalized cuts and image segmentation. *IEEE Trans. Pattern Analysis and Machine Intelligence*, 22(8):888–905, 2000.

[17] O. Veksler, Y. Boykov, and P. Mehrani. Superpixels and supervoxels in an energy optimization framework. In *Europeon Conference on Computer Vision (ECCV '10)*, pages 211–224, 2010.

[18] P. Wang, G. Zeng, R. Gan, J. Wang, and H. Zha. Structure-sensitive superpixels via geodesic distance. *International Journal of Computer Vision*, 103(1):1–21, 2013.

[19] S. Wang, H. Lu, F. Yang, and M.-H. Yang. Superpixel tracking. In *IEEE International Conference on Computer Vision (ICCV '11)*, pages 1323–1330, 2011.

[20] X. Wang, X. Ying, Y.-J. Liu, S.-Q. Xin, W. Wang, X. Gu, W. Mueller-Wittig, and Y. He. Intrinsic computation of centroidal Voronoi tessellation (CVT) on meshes. *Computer-Aided Design*, 58:51–61, 2015.

[21] C.-C. Yu, Y.-J. Liu, T. Wu, K.-Y. Li, and X. Fu. A global energy optimization framework for 2.1d sketch extraction from monocular images. *Graphical Models*, 76(5):507–521, 2014.